RFI mitigation with the time-frequency robust statistical analysis

P. A. Fridman,

ASTRON, Postbus 2, 7990AA, Dwingeloo, The Netherlands,
email: fridman@astron.nl

Abstract

The real sensitivity of radio astronomical stations is often limited by man-made radio emissions, radio frequency interference (RFI) due to activities such as broadcasting operations, radars, and a variety of communication and radiolocation systems. Time-frequency analysis with high temporal and frequency resolution allows us to detect and excise RFI better than can be done with existing standard radiotelescope backends. The statistical errors of the total power, correlation factor and spectral density may be substantially reduced when robust statisitical methods are applied to data.

1 Introduction

Radio frequency interference (RFI) substantially limits a radiotelescope's real sensitivity, [1-10]. Several methods of RFI mitigation have recently been proposed [11-33]. These methods can be applied both to existing radiotelescopes and to future projects, [34-37]. One of the main tools of **real-time** RFI mitigation is the time-frequency analysis of received signals with a high temporal (less than 1 microsecond) and frequency (less than 1 kiloHertz) resolution. This approach allows us to analyze statistics of the mixture "system noise + source noise + RFI" and to separate RFI from the Gaussian probability distribution function of the "system noise + source noise". Application of modern, robust, statistical methods to the non-Gaussian RFI mitigation problem is considered in this paper.

2 Conventional measurement schemes

There are three main types of radioastronomical statistical measurements:
a) measurement of variance or total power (making a map with a single dish, or pulsar observations);
b) measurement of correlation function (aperture synthesis, polarization observations);
c) measurement of power spectrum (spectral line observations).

2.1 Total power measurements

Figure 1 illustrates the simplified scheme of a single dish radio telescope with a total power radiometer at the output. In the absence of RFI the sum "system noise + source noise" is random noise with a Gaussian probability density function (PDF), zero mean and variance equal to the sum of the system noise's variance and the source noise's variance. For n independent "clean"(no RFI) samples $x_1, x_2, ...x_n$, (upper waveform), their joint PDF is the product $L(x \mid \sigma) = p(x_1 \mid \sigma)p(x_2 \mid \sigma)...p(x_n \mid \sigma) = \prod_{i=1}^{n} \frac{1}{\sigma\sqrt{2\pi}} \exp(-\frac{x_i^2}{2\sigma^2})$, where σ is the parameter to be measured. Classical statistics gives the Maximum Likelihood (ML) estimate σ_0 which is the solution of the equation:

$$\sum_{i=1}^{n} \frac{\partial}{\partial \sigma} \log L(x_i, \sigma) \mid_{\sigma=\sigma_0} = 0. \tag{1}$$

Therefore, for the Gaussian PDF, $\widehat{\sigma_0^2} = \frac{1}{n}\sum_{i=1}^{n} x_i^2$, which is precisely the output of the total power detector (TPD). This value is proportional to the sum: system temperature + source antenna temperature, $\widehat{\sigma^2} \sim T_{sys} + T_a$. But in the presence of RFI, (lower waveform), the TPD output will be substantially different.

2.2 Correlation function

Figure 2 illustrates the simplified scheme of a two-element radio-interferometer. The bivariate Gaussian PDF for each pair of samples from the two sites in the absence of RFI is

$$p(x,y) = \frac{1}{\sqrt{2\pi\sigma_1\sigma_2(1-r^2)}} \exp[-\frac{1}{2(1-r^2)}(\frac{x^2}{\sigma_1^2} - 2r\frac{x}{\sigma_1}\frac{y}{\sigma_2} + \frac{y^2}{\sigma_2^2})]. \tag{2}$$

3 Several examples

Several examples of computer simulations of radioastronomical observations with RFI are given in this subsection. Figures 3, 4, 5, 6 all have the same structure: (a) a sample of "clean" Gaussian noise (no RFI); (b) a set of estimates derived from successive samples of "clean" noise, which correspond to an "off-source ⇒ on-source ⇒ off-source" observational set; (c) a sample with strong burst-like RFI; (d) the comparable set of estimates derived from the contaminated noise, which produces no visible "on-source" step; (e) the set of comparable estimates provided by a robust statistical algorithm (which will be specified in the following sections).

These figures obviously show that the ordinary backend processing (section 2), which is optimal for a Gaussian PDF, works extremely badly for a contaminated Gaussian PDF:

$$P_\epsilon(x, \sigma_0, \sigma_1) = (1 - \epsilon)P(x, \sigma_0) + \epsilon P(x, \sigma_1), 0 < \epsilon < 1, \tag{6}$$

where $P(x, \sigma_0)$ is the "clean" PDF, σ_0 is the parameter to be measured, $P(x, \sigma_1)$ is the contaminating PDF, ϵ characterizes the fraction of $P(x, \sigma_1)$ in the total $P_\epsilon(x, \sigma_0, \sigma_1)$.

There are several ways to characterize the robustness of a statistical procedure. One of the most adopted is the **influence function**.

4 Influence function

Let $T = \{T_n\}$ be a sequence of estimates of a parameter θ. $T_n(X)$ denotes the estimate made from the samples $X = (x_1, ...x_n)$ and $T_{n+1}(x, X)$ denotes the same estimate based on the sample $(x, x_1, ...x_n)$, that is one more sample x is added. The influence function (IF) is defined as

$$\varphi_n(x, X) = T_{n+1}(x, X) - T_n(X). \tag{7}$$

This function characterizes the sensitivity of the estimate T_n to the adding of one sample x. For example, the IF for the sample mean $T_n = \frac{1}{n}\sum_{i=1}^{n} x_i$ is

$$\varphi_n(x, X) = \frac{x}{n+1} - \frac{1}{n(n+1)}\sum_{i=1}^{n} x_i = \frac{x}{n+1} + O(\frac{\mu}{n}). \tag{8}$$

Therefore, the IF is not bounded, and an outlier can cause an unbounded error.

The IF for the sampled variance is

$$\varphi_n(x, X) = \frac{x^2 - \widehat{\sigma_n^2}}{n+1}, \tag{9}$$

that is for $|x| < \sigma_n$ the estimate is slightly reduced, but when $|x| \to \infty$, the error grows very rapidly following the square law.

The next section is dedicated to **robust algorithms** which are less susceptible to the outliers, and the IF for these algorithms is given.

5 Robust algorithms

5.1 Nonparametric statistics

One of the simplest methods to overcome the lack of robustness is to analyze the "heavy tails" of the contaminated sample PDF (6). Let $(x_1, ...x_n)$ be a sample consisting of n independently observed values of a random variable x with a PDF $P(x)$. If we arrange the x in increasing order (denoting the smallest by $x^{(1)}$, the next smallest by $x^{(2)}$, etc.),

$$x^{(1)} < x^{(2)} < ... < x^{(n)},$$

then we call each of them an *order statistic*. Let $r = r_1 + r_2$ order statistics from the tails be thrown away, so that the estimate of a parameter will be based on the remained samples

$$x^{(r_1+1)} < x^{(r_1+2)} < ... < x^{(n-r_2)}.$$
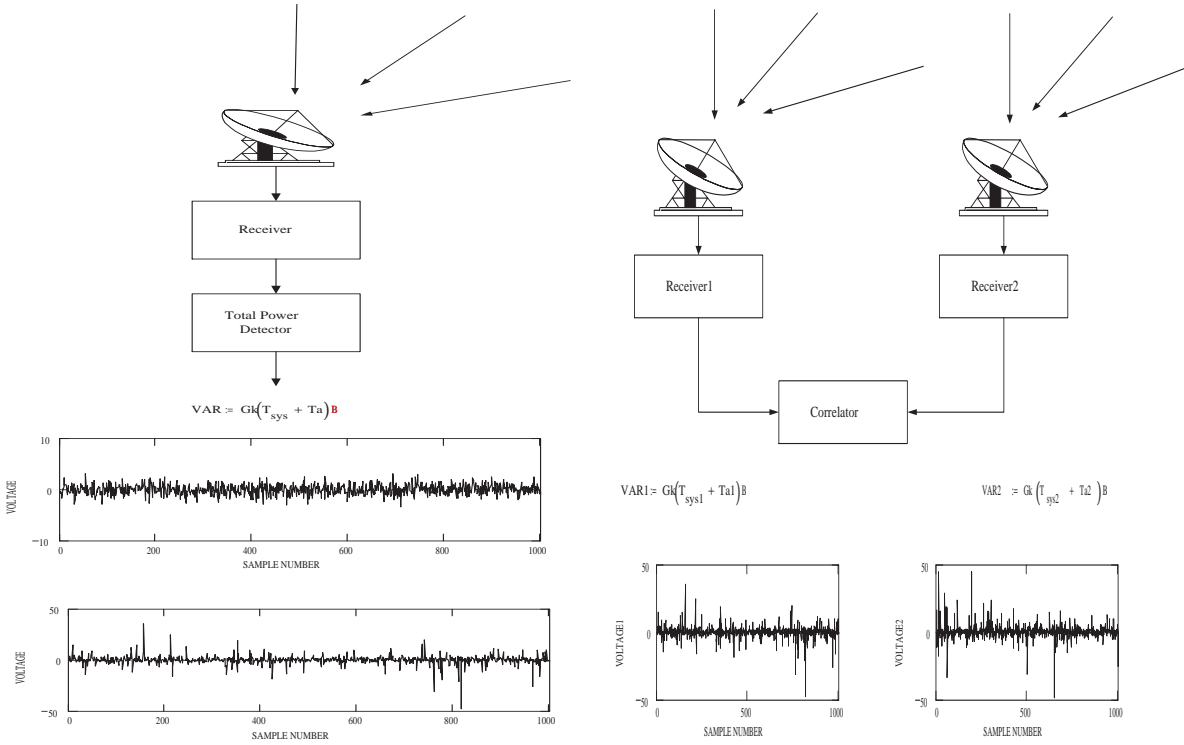
Fig. 1, (left panel). Single dish radiotelescope with the total power detector at the output, VAR is the variance of the noise at the receiver output in the absence of RFI, T_{sys} and T_a are the system and radio source antenna temperature, respectively, G is the receiver gain, B is the bandwidth. The waveforms illustrate the receiver's voltage output without and with RFI (before the total power detector and correlator).

Fig. 2, (right panel). Radio interferometer with the correlator at the output.

The ML estimates of the correlation factor r and the variances σ_1^2, σ_2^2 are

$$\widehat{r} = \frac{\frac{1}{n}\sum_{i=1}^{n} x_i y_i}{\sqrt{\widehat{\sigma_1^2}\widehat{\sigma_2^2}}}, \tag{3}$$

$$\widehat{\sigma_1^2} = \frac{1}{n}\sum_{i=1}^{n} x_i^2, \quad \widehat{\sigma_2^2} = \frac{1}{n}\sum_{i=1}^{n} y_i^2, \tag{4}$$

which are not statistically stable (**robust**) in the presence of outliers from RFI, as in the waveforms of Fig. 2.

2.3 Power spectrum

The power spectrum is measured during spectral-line observations using either the autocorrelation function (after a Fourier transform, with the XF spectrometer), or directly after averaging M instantaneous spectral densities at the receiver output (FX spectrometer):

$$\widehat{S(k)} = \frac{1}{M}\sum_{m=0}^{M-1}\{[\sum_{n=0}^{N-1} x_n cos(2\pi n\frac{k}{N})]^2 + [\sum_{n=0}^{N-1} x_n sin(2\pi n\frac{k}{N})]^2\} \tag{5}$$

This estimate is statistically unstable (sensitive to the outliers) as well.
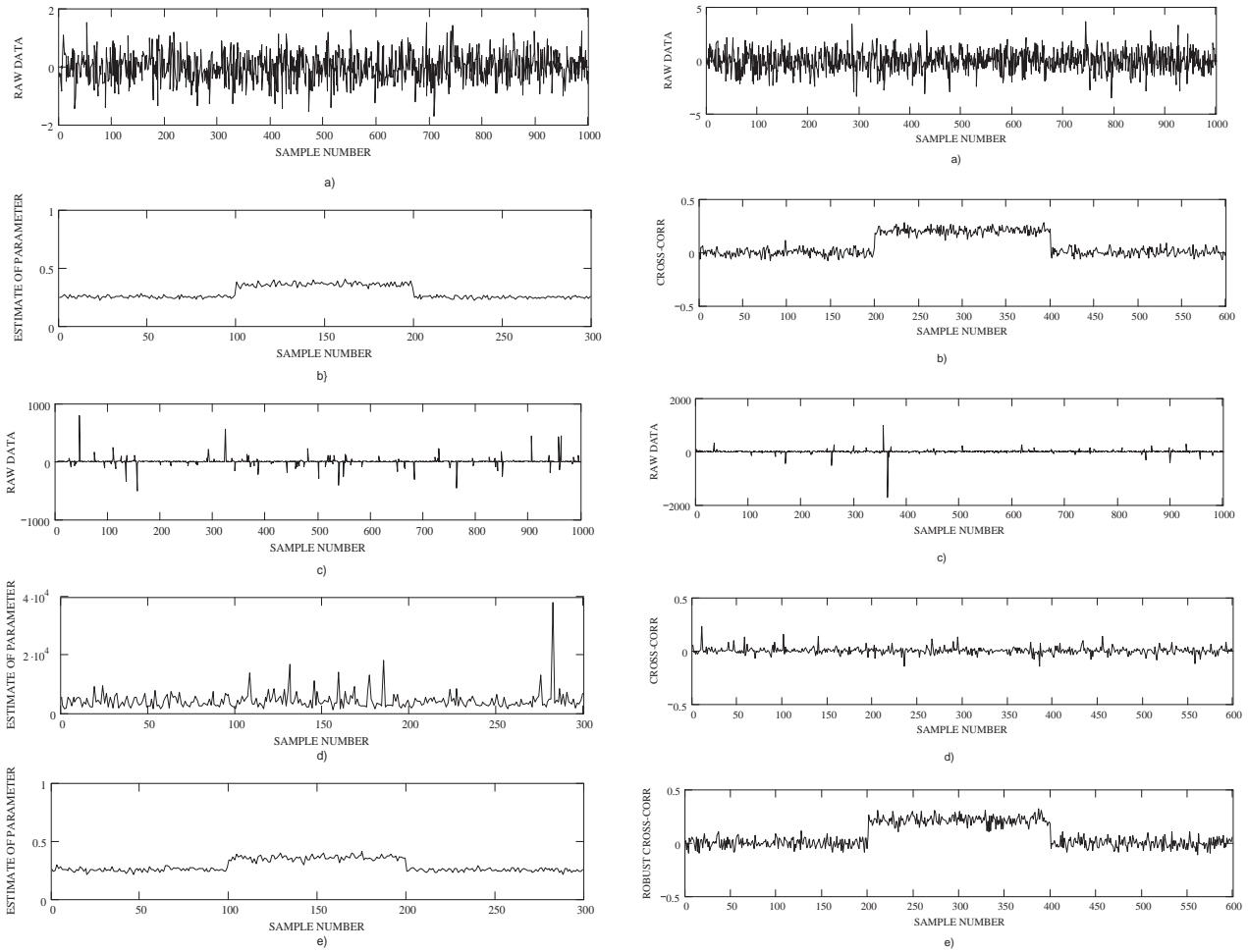
Fig. 3 (left panel). a) Noise with a the Gaussian PDF, $\mu = 0, \sigma = 0.5$, and no interference.

b) Estimate of the variance $\widehat{\sigma^2}$ of the Gaussian PDF (sample variance) at 300 points, each point being the estimate derived from n=1000 samples of the noise stream illustrated in Fig. 3a. Two steps at M1=100 and M2=200 ("on source", $\Delta\sigma = 0.1$) are visible.

c) Noise with a Gaussian PDF, $\mu = 0, \sigma = 0.5$, and interference: random impulses from a Poisson distribution ($\lambda_p = 0.05$) and lognormal distribution of amplitudes (mean=2R, standard deviation =1R, R=10) replace some variates. Note the vertical scale, which is 500 times larger than in Fig. 3a.

d) Estimate of the variance $\widehat{\sigma^2}$ of the Gaussian distribution (sample variance) at 300 points, each point is the estimate from n=1000 samples of the noise stream illustrated in Fig. 3c. No change of the mean is visible; the standard deviation = 1824 is 12680 times larger than in Fig. 3b.

e) Robust estimation of the variance $\widehat{\sigma^2}$ of a Gaussian PDF at 300 points, each point being the estimate from n=1000 samples of the noise stream illustrated in Fig. 3c. Two steps at M1=100 and M2=200 ("on source", $\Delta\sigma = 0.1$) are clearly visible. Standard deviation of the averaged data = 0.014.

Fig. 4 (right panel). a) Noise with a Gaussian PDF, $\mu = 0, \sigma = 1$, and no interference.

b) Cross-correlation function of two signals like that in Fig. 4a with a coherent component $\Delta\sigma = 0.5$ between points M1=200 and M2=400 ("on-source"); each point corresponds to the estimated cross-corr derived from 1000 sequential variates in the data stream illustrated by Fig. 4a.

c) Noise with a Gaussian probability distribution, $\mu = 0, \sigma = 1$, and interference: random impulses from a Poisson distribution ($\lambda_p = 0.05$) and lognormal distribution of the amplitudes (mean = 2R, standard deviation = 1R, R=10) replace some variates. Note that the vertical scale is 400 times larger than in Fig. 4a.

d) Cross-correlation function of two signals like that illustrated by Fig. 4c, with a coherent component $\Delta\sigma = 0.5$ between M1=200 and M2=400 ("on-source"); each point corresponds to the estimate from 1000 variates. No change in the cross-correlation coefficient is visible.

e) Robust cross-correlation function of the two signals with RFI and a coherent component $\Delta\sigma = 0.5$ between points M1=200 and M2=400; each point corresponds to the estimate derived from 1000 variates. The steps at M1=200 and M2=400 are clearly visible, though the standard deviation is slightly larger than in the absence of interference.

201
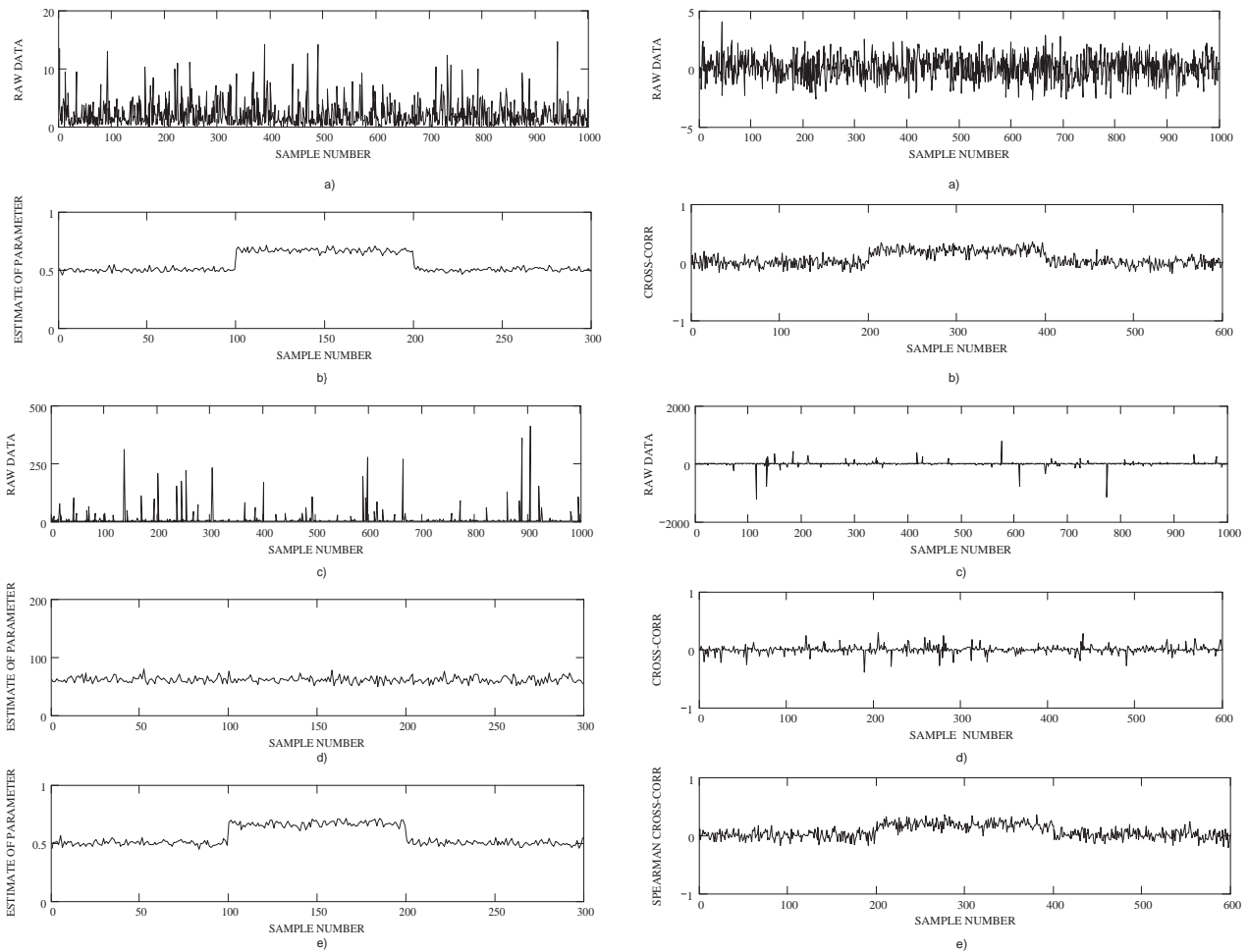
Fig. 5 (left panel). a) Noise with an exponential probability distribution, $\lambda_e = 2.0$, and no interference.

b) Estimate of the λ_e of the exponential distribution (sample mean) at 300 points, each point being the estimate from n=1000 samples of the noise illustrated in Fig. 5a.

c) Noise with an exponential probability distribution, $\lambda_e = 0.5$, and interference, together with random impulses from a Poisson distribution ($\lambda_p = 0.05$) and lognormal distribution of the amplitudes (mean=2R, standard deviation =1R, R=10). Note the vertical scale is 20 times larger than in Fig. 5a.

d) Estimate of the λ_e of the exponential distribution (sample mean) at 300 points, each point being the estimate from n=1000 samples of the noise stream illustrated in Fig. 5c. There is no visible change of the mean. The standard deviation = 4.841, which is 177 times larger than in Fig. 5b.

e) Robust estimate of the λ_e of the exponential distribution (mean) at 300 points, each point being the estimate from n=1000 samples of the noise in Fig. 5c. The two steps at M1=100 and M2=200 ("on-source", $\Delta\lambda_e = 0.5$) are clearly visible. Standard deviation of the averaged data = 0.027.

Fig. 6 (right panel). a) Noise from a Gaussian PDF, $\mu = 0, \sigma = 1$, and no interference.

b) Cross-correlation function of two signals with a coherent component $\Delta\sigma = 0.5$ between M1=200 and M2=400 ("on-source"); each point corresponds to the estimated cross-corr derived from 200 sequential variates in the data stream illustrated by Fig. 6a.

c) Noise with a Gaussian probability distribution, $\mu = 0, \sigma = 1$, and interference: random impulses from a Poisson distribution ($\lambda_p = 0.05$) and lognormal distribution of the amplitudes (mean = 2R, standard deviation = 1R, R=10) replace some variates. Note the vertical scale is 400 times larger than that in Fig. 6a.

d) Cross-correlation function of two signals like those of Fig. 6c, with a coherent component $\Delta\sigma = 0.5$ between M1=200 and M2=400 ("on-source"); each point corresponds to the estimate from 200 samples from the noise stream of Fig. 6c. There is no visible change in the cross-correlation coefficient.

e) Spearman rank cross-correlation function of two signals like that of Fig. 6c with a coherent component $\Delta\sigma = 0.5$ between M1=200 and M2=400: each point corresponds to the estimate from 200 samples dreawn from a noise stream like Fig. 6c. The steps at M1=200 and M2=400 are clearly visible, and the standard deviation is practically the same as in the absence of interference.

202

The samples are thus *censored*. Two options are possible [41]:

1. *Trimming*: all measurements outside the interval $[x^{(r_1+1)}, x^{(n-r_2)}]$ are removed.

2. *Winzorisation*: the "left tail" is pulled to the value $x^{(r_1+1)}$, so that all $x < x^{(r_1+1)}$ are equated to $x^{(r_1+1)}$, and the "right tail" is likewise pulled to the value $x^{(n-r_2)}$. The mean, variance and other parameters are calculated with the remained samples. The estimate functions and the influence functions for the trimmed, winzorized and ordinary variance are given in Fig. 7 and 8 respectively. The *trimmed* and *winzorized* estimates are more robust, and the corresponding IFs are bounded.

If n is odd, that is $n = 2m - 1$, then the middle value $x^{(m)}$, or else, the sample *median*, is also a robust estimate of the mean for symmetrical PDF, and the median deviation around the sample median

$$s_2 = median_{1 \le i \le n}\{|x_i - median_{1 \le i \le n}\{x_i\}|\}/0.6745 \tag{10}$$

also has good robustness.

5.2 M-estimates

A more universal approach was proposed in [38]. In general, the estimate of a PDF's parameter θ is the value $\widehat{\theta}$ minimizing the sum

$$\sum_{i=1}^{n} \rho(x_i, \widehat{\theta}) \to min, \tag{11}$$

where $\rho(x_i, \widehat{\theta})$ is a continuous and differentiable function on x and $\widehat{\theta}$. For example, for the mean $\rho(x - \widehat{x}) = (x - \widehat{x})^2$, and for the median $\rho(x - med) = |x - med|$. After the differentiation of (11) with respect to $\widehat{\theta}$ we get

$$\sum_{i=1}^{n} \Psi(x_i, \widehat{\theta}) = 0, \tag{12}$$

where the anti-symmetric function Ψ is called a *score function* and the estimate is called an **M-estimator**. Again for the mean $\Psi(x - \widehat{x}) = x - \widehat{x}$, and for the median $\Psi(x - med) = sgn(x - med)$. The influence function for the M-estimator has a form:

$$\varphi(x) = \frac{\Psi(x - \hat{\theta})}{\Psi'(x - \hat{\theta})}. \tag{13}$$

The maximum likelihood (ML) estimate corresponds to $\rho(x) = -log[p(x)]$, where $p(x)$ is the PDF.

The score function Ψ for the estimate of a mean was found [38] for the worst contaminating "heavy-tailed" symmetric PDF (Laplace PDF) to be

$$\Psi_{Huber}(x - \hat{\theta}) = \begin{cases} -k, \text{ if } x - \hat{\theta} < k, \\ x - \hat{\theta}, \text{ if } -k \le x - \hat{\theta} \le k, \\ k, \text{ if } k < x - \hat{\theta} \end{cases} \tag{14}$$

where k depends on ϵ in the following way:

$$\frac{1}{1 - \epsilon} = 1 - 2\Phi(-k) + \frac{2}{k}p(k), \text{ and } \Phi(z) = \int_{-\infty}^{z} p(x)dx, \tag{15}$$

$p(x)$ is the Gaussian PDF with zero mean and a variance of 1. Several other functions $\Psi(x)$ for the robust

estimates were proposed, [40, 41, 42]:

$$\Psi_{Andrews}(x) \quad = \quad \begin{cases} sin(x/a) \text{ if } |x| \le a\pi, \\ 0 \qquad \text{if } |x| > a\pi \end{cases} \quad ; \tag{16}$$

$$\Psi_{Hampel}(x) \quad = \quad \begin{cases} x \text{ if } |x| \le a \\ a \times sign(x) \text{ if } a < |x| \le b \\ \frac{a \times sign(x)(c-|x|)}{c-b} \text{ if } b < |x| \le c \end{cases} \quad ; \tag{17}$$

$$\Psi_{Tukey}(x) \quad = \quad \begin{cases} 0 \text{ if } |x| > c \\ x(1-x^2)^2 \text{ if } |x| < 1 \\ 0 \text{ if } |x| \ge 1 \end{cases} \quad ; \tag{18}$$

$$\Psi_{Meshalkin}(x) \quad = \quad x \times exp(-\lambda x^2/2), \lambda > 0. \tag{19}$$

The parameters a, b, c, λ are tuned for the particular contaminated PDF (6). Fig. 7 gives the estimate functions of the variance for the three cases: Maximum Likelihood (nonrobust), Huber (14), and Meshalkin (19), while Fig. 8 illustrates the corresponding influence functions.

Now we can go to the low panels in Fig. 3, 4, 5, 6, where the simulation results are given for the robust estimates.

Figure 3e illustrates application of robust estimation to the variance $\widehat{\sigma^2}$ of the Gaussian PDF. With the assumption that the mean is equal to zero, the estimate equation (12) is

$$\sum_{i=1}^{n}(\frac{x_i^2}{\sigma^2} - 3/5)exp(-x_i^2/3\widehat{\sigma^2}) = 0. \tag{20}$$

The steps due to the "off-source → on-source → off-source" are clearly visible, while the input data x_i were taken from the data stream illustrated by Fig. 3c.

Figure 4e illustrates the advantage of robust processing in the case of a correlator (Fig. 2). The cross-correlation coefficient between random samples $x1_i$ and $x2_i$ is calculated with

$$\widehat{r_{12}} = \frac{1}{n\sqrt{\widehat{\sigma1^2}\widehat{\sigma2^2}}} \sum_{i=1}^{n} x1_i \exp(-\frac{x1_i^2}{3\widehat{\sigma1^2}})x2_i \exp(-\frac{x2_i^2}{3\widehat{\sigma2^2}}), \tag{21}$$

where the robust estimates of $\widehat{\sigma1^2}$ and $\widehat{\sigma2^2}$ were found using (20), and each product $x1_ix2_i$ is exponentially weighted: the larger the variate, the lower its weight, thus eliminating the outliers.

Figure 5e shows the robust estimatation of the power spectrum at the output of an FX spectrometer (instead of the straight averaging of (5)). The root of the following equation yields the estimate of the parameter λ_e of an exponential PDF [42]:

$$\sum_{i=1}^{n}(\frac{x_i}{\lambda_e} - 2/3)exp(-\frac{x_i}{2\lambda_e}) = 0. \tag{22}$$

Figure 6e illustrates the application of a nonparametric procedure, Spearman's rank-order correlation coefficient [43]. The *ranks* ξ_i and η_i of the samples $x1_i$ and $x2_i$ are their numbers in the order statistics (see subsection 5.1). The Spearman's rank-order correlation coefficient is calculated from the ranks instead of the variates (as in (3)) via

$$R = \frac{3\sum_{i=1}^{n}(2\xi_i - n - 1)(2\eta_i - n - 1)}{n(n-1)(n+1)}. \tag{23}$$

A significant improvement in the outcome is clearly visible in Fig. 6e.
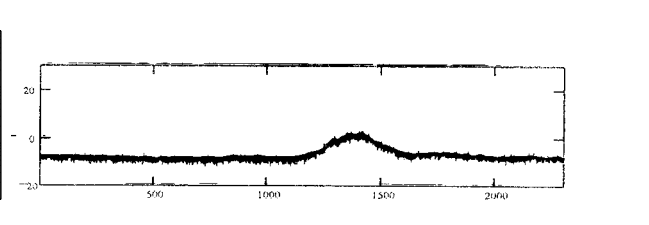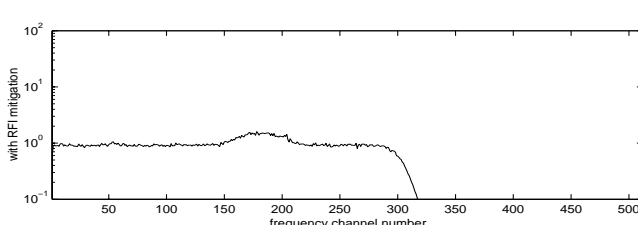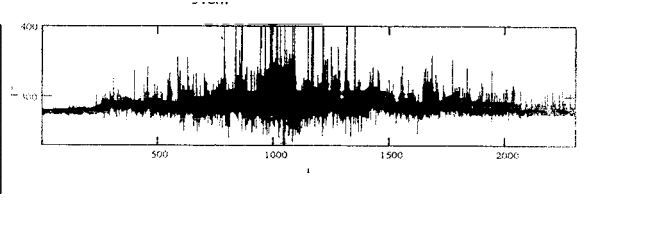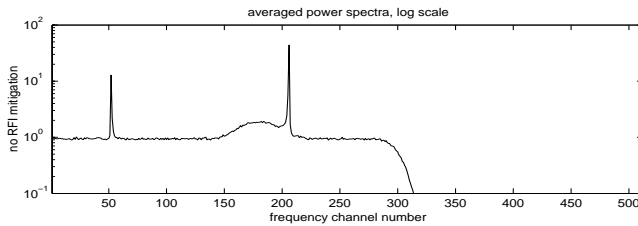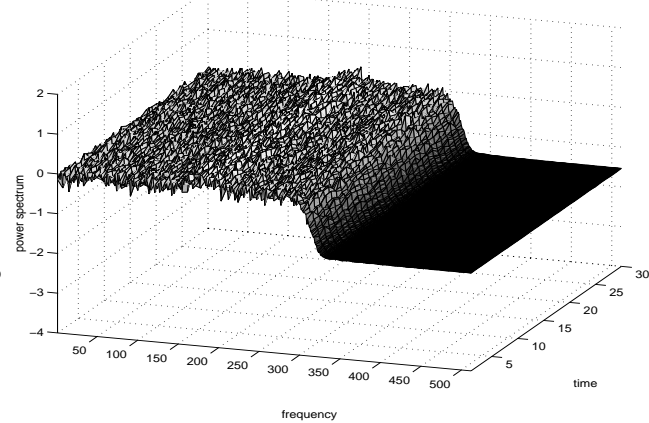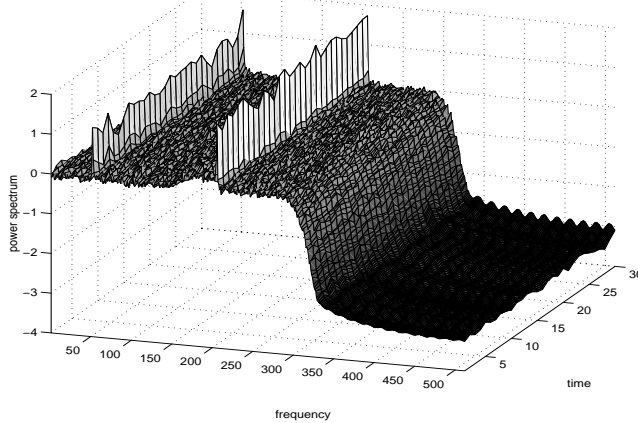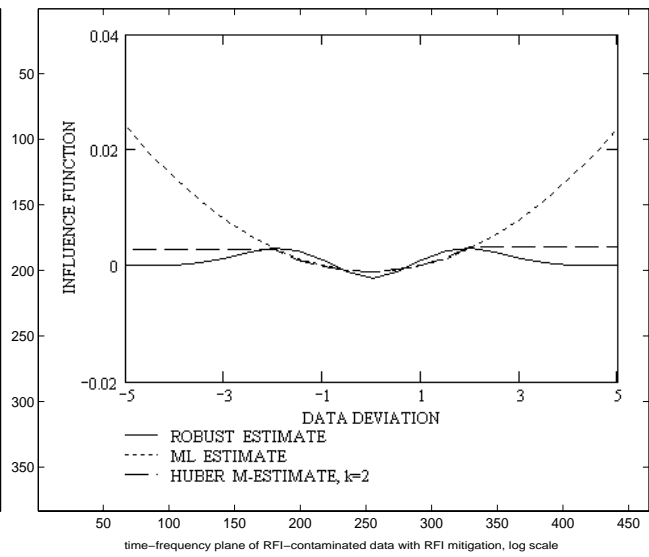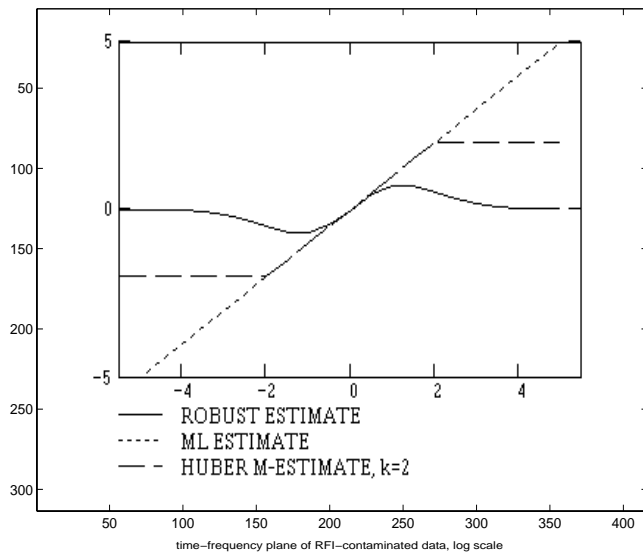
Fig. 7, (top left). Score functions for the Gaussian PDF, $\mu = 0, \sigma = 1.0$.

Fig. 8 (top right). The influence functions corresponding to Fig. 7.

Fig. 9, (middle left). Time-frequency 3D-presentation of the power spectrum with system noise, RFI and spectral lines, from a computer simulation using equation 5.

Fig. 10, (middle right). Time-frequency 3D-presentation of the robustly estimated power spectrum, which suppresses RFI: the spectral line is visible.

Fig. 11, (bottom left). The averaged power spectra corresponding to Fig. 9 (upper panel) and to Fig. 10 (lower panel).

Fig. 12, (bottom right). Real observations at RATAN-600, $\lambda = 31cm$, 20.08.1996, scan of the source 1116+28, upper panel - with RFI and without RFI excision,

lower panel - the same radio source with outliers excised before averaging, both records were made simultaneously.
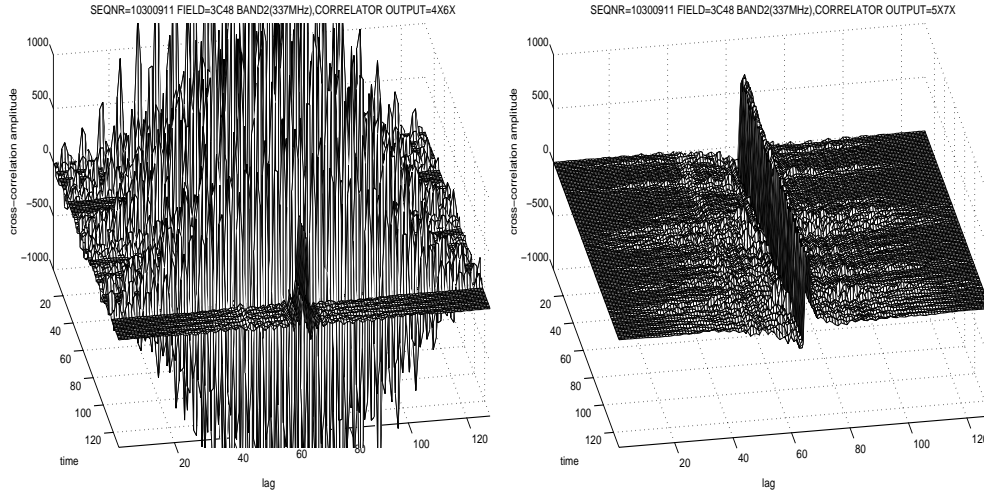
Fig. 13. Observation at WSRT n.10300911, 29 Jan 2003, source 3C48, frequency 337 MHz, bandwidth 10 MHz, DZB correlator, 60 s integration time for each of 131 records ($\approx 2h$). RFI was suppressed at channels RT5X and RT7X, but not suppressed at channels RT4X, RT6X. The time-frequency presentations of the **cross-correlation amplitudes** are given: 4X6X - left panel, 5X7X - right panel.

These algorithms work well with RFI bursts in the temporal domain, but they do not "see" narrow-band RFI, which is sometimes hidden under the system noise. On the other hand RFI of this type can be easily detected in the frequency domain as bursts above the level of the system noise spectral power density, and a robust algorithm can be applied in the frequency domain. It is worth remembering here that the power density calculated after the Fourier transform of one sequence of sample data, see (5), for $M = 1$, has an exponential PDF for each frequency bin, when the PDF of noise in the temporal domain is Gaussian. Figures 9, 10 & 11 illustrate the application of the robust Meshalkin procedure [42] to the estimation of the parameter λ_e in the exponential PDF. The solution of equation (12) has the score function

$$\Psi(x) = (\frac{x}{\lambda_e} - 2/3)e^{-x/2\lambda_e}. \tag{24}$$

RFI was simulated as sequences of a continuous wave with two different frequencies and random start times and amplitudes. The signal of interest is represented as a "spectral line": narrow-band noise is superposed with the system noise. Fig. 9 shows the 3D-presentation of the time evolution of the power spectrum with RFI that was calculated using equation 5: each section corresponds to the averaging of $M = 50$ spectra, and the number of frequency channels is 512 ($N = 1024$). Fig. 10 is the 3D-presentation of the sequence of the robustly estimated power spectra, and Fig. 11 gives the averaged spectra on a logarithmic scale, corresponding to Figs. 9 & 10: upper panel is the averaged spectrum without robust processing; the lower panel illustrates the averaged spectrum obtained after using a robust algorithm.

It should be noted that there are always certain losses after the application of robust algorithms. The variance of the robust estimate is, as a rule, higher than that for the "ideal" case (no RFI and ML algorithm), and the ratio of the estimation variances can achieve 1.5-2 in favour of the "ideal" case. But in the presence of strong RFI, these losses are more tolerable than the total loss of the observations.

Figures 12 and 13 show examples of real-time signal processing (trimming) applied during observations at RATAN-600 and WSRT, respectively. Figure 12 illustrates RFI mitigation with a total power detector: $\lambda = 31cm$, 20.08.1996, source 1116+28 is scanned by the radio telescope antenna pattern; upper panel - with RFI and without RFI excision, lower panel - the same radio source with RFI excision, both records were made simultaneously. The primary sampling interval (before averaging) was equal to 2 μs, the final averaging interval is equal to 0.1 ms.

Figure 13 illustrates RFI mitigation with a radio interferometer, where cross-correlation is measured: source 3C48, frequency 337 MHz, bandwidth 10 MHz, DZB correlator, 60 s integration time for each of the 131 records ($\approx 2h$). RFI was suppressed in the frequency domain at channels RT5X and RT7X and not suppressed at channels RT4X, RT6X. The time-frequency presentations of the **cross-correlation amplitudes** are given: 4X6X - left panel, 5X7X - right panel. The right panel illustrates the effect of RFI suppression.

Figures 12 and 13 thus show that even simple, real time algorithms can give significant benefits.

6   Conclusions

1. Existing radio telescope backends process signals following classic maximum likelihood statistical algorithms, which are optimal for a no-RFI environment. These procedures are not robust: they are statistically unstable in the presence of outliers in the time or frequency domains, or, in other words, when the PDF is contaminated.

2. Algorithms, developed to provide robust or nonparametric statistical output are more suited to our worsening RFI situation. They also provide a much more acceptable level of residual errors in the presence of strong RFI.

3. The implementation of real-time robust algorithms requires more computational power than is used in existing backends. The high performance of modern digital signal processing components (processors (DSP), field programmable gate arrays (FPGA)) permit, however, the **real-time** implementation of many efficient robust procedures. It is not always possible to combine such processing with existing radiotelescope infrastructure, but future backends should be designed to implement robust algorithms.

7   References

[1] J. Galt, "Contamination from Satellites", *Nature*, 345, p. 483 (1990).

[2] A. R. Thompson, T. E. Gergely and P.A. Van den Bout, "Interference and Radioastronomy", *Physics Today*, Nov. 1991, pp. 41-49.

[3] W. L., Combrinck, M.E., West, M. J. Gaylard, "Coexisting with GLONASS", *Publ. Astronomical Society of the Pacific*, 106, 807-812, July 1994.

[4] J. Maddox, Radio Astronomy and Unquiet Radio Sky, *Nature*, 378, p. 11 (1995).

[5] CRAF Handbook for Radio Astronomy, 2-nd ed., Committee on Radio Astronomy Frequencies of European Science Foundation, 1997.

[6] T. A. Th. Spoelstra, "Will Radio Astronomy Survive?" *Tijdcshrift van het Nederlands Electronica- en Radiogenootschap*, 62. n.1, pp.13-17, 1997.

[7] J. Roth , "Will the Sun Set on Radio Astronomy?", *Sky & Telescope*, 94, n. 4, pp. 41-44, April 1997

[8] J. Cohen, "Radio pollution: the invisible threat to radio astronomy", *Astronomy & Geophysics*, 40, n. 6, pp. 8-13, Dec. 1999.

[9]. J. Schenker, "Hidden by Radio Smog", *Time*, July 1999, p. 46.

[10] H. C. Kahlmann, "The Limits of Radio Astronomy", in *Review of Radio Science 1996-1999*, ed. W. Ross Stone (URSI: Oxford University Press), pp. 751 - 789, 1999.

[11] C. Barnbaum, R. F. Bradley, "A New Approach to Interference Excision in Radio Astronomy: Real-Time Adaptive Cancellation", *Astronomical J.*, 115, 2598-2614, Nov. 1998.

[12] A. Leshem, A-J. van der Veen, A-J. Boonstra, "Multichannel Interference Mitigation Techniques in Radio Astronomy", *Astrophysical J. Suppl. Series*, 131, pp. 355-373, Nov. 2000.

[13] F. H. Briggs, J. F. Bell, M. J. Kesteven, "Removing Radio Interference from Contaminated Astronomical Spectra using an Independent Reference Signal and Closure Relations", *Astronomical J.*, 120, pp. 3351-3361, Dec. 2000.

[14] S. W. Ellington, J. D. Bunton, J. F Bell, "Removal of the Glonass C/A Signal from OH Spectral Line Observations Using a Parametric Modeling Technique", *Astrophysical J. Suppl.*, 135, pp. 87-93, July 2001.

[15] R. Weber, C. Faye, F. Biraud and J. Dansou, "Spectral detector for interference time blanking using quantized correlator", *Astronomy & Astrophysics, Suppl. Ser.*, 126,pp. 161-167, 1997.

[16] The Elizabeth and Frederick White Conference on Radio Frequency Interference Mitigation Strategies, 15 - 16 December 1999, CSIRO Radiophysics Laboratory, Sydney, Australia, *http : //www.atnf.csiro.au/SKA/intmit/atnf/conf*.

[17] The RFI-MitigationWorkshop cosponsored by IUCAF, IAU (Division X, RFI Mitigation Working Group), EC-ICN, (Infrastructure Cooperation Network in Radio Astronomy), MPIfR (Max-Planck-Institut fur Radioastronomie), 28th to 30th March, 2001, *http : //www.mpifr − bonn.mpg.de/staff/kruf/iucaf/RFI.htm*.

[18] P. A. Fridman, "Radio frequency interference rejection in radio astronomy", *Astronomy & Astrophysics*

Transactions, 19, n. 3-4, pp. 624-645, 2000).

[19] P. A. Fridman "RFI excision using higher order statistics of the power spectrum", *Astronomy & Astrophysics*, 368, pp. 369-376, 2001.

[20] P. A. Fridman and W. A. Baan , "RFI mitigation methods in radio astronomy", *Astronomy & Astrophysics*, 378, n1, pp. 327-344, (October IV 2001).

[21] P. A. Fridman, "Robust power spectrum estimation in the presence of interferences", in *Signal and Data Processing of Small Targets*, SPIE, v. 4473, pp. 1-12, San-Diego, 31 July-3 Aug., 2001.

[22] P. Fridman, "DSP experimental system for radio frequency interference mitigation at WSRT", *ASTRON*, ITR- 221, pp. 1- 250, 2000.

[23] P. A. Fridman, "Radio Frequency Interference and Possible Counteract Methods in Radio Astronomy Receivers", *Proc. of Workshop on Large Antennas in Radio Astronomy*, Feb. 28-29, 1996, ESTEC, Noordwijk, The Netherlands, pp. 59-67.

[24] P. A. Fridman, "Time-Frequency Analysis of Electromagnetic Pollution in Radio Astronomy Receivers", *Proc. of IEEE-SP International Symposium on Time-Frequency and Time-Scale Analysis*, June 18-21, 1996, Paris, France, pp. 365-367.

[25] P. A. Fridman, "A Change Point Detection Method for Elimination of Industrial Interference in Radio Astronomy Receivers", *Proc.of 8th IEEE Signal Processing Workshop on Statistical Signal and Array Processing*, June 24-26, 1996, Corfu, Greece, pp. 264-266.

[26] A. B. Berlin, P. A. Fridman, "Real-Time Radiometric Data Processing against Electromagnetic Pollution", *Abstracts of the XXVth General Assembly of the International Union of Radio Science*, Aug. 28 - Sept.5, 1996, Lille, France, p. 750.

[27] A. B. Berlin, E. V. Bulaenko, P. A. Fridman, "RFI suppression device for RATAN-600 radiometer at 13cm", *Problems of modern radioastronomy*, v.3, pp. 158-159, 1997, (in Russian).

[28] P. A. Fridman, "Radio frequency interference rejection in radio astronomy receivers", *NFRA Note 664, (EVN Doc 97)*, pp. 1-35, Dec. 1997.

[29] P. A. Fridman, E. V. Bulaenko, S. V. Tuzenko, "Radio Frequency Interference Suppression in Radio Astronomy by Real-Time Digital Signal Processing", *Proceedings of the First International Conference and Exhibition, Digital Signal Processing and its Applications*, June 30-July 3, 1998, Moscow, Russia, pp. III-E-55-66.

[30] P. A. Fridman, "Radio Frequency Interference Rejection in Radio Astronomy Receivers", *Signal Processing IX, Proceedings of EUSIPCO-98 Ninth European Signal Processing Conference*, Rhodes, Greece, 8-11 September 1998, pp. 2241-2243.

[31] P. A. Fridman , "DSP Experimental System for Radio Frequency Interference Mitigation at Radio Telescope", *Proceedings of the IEEE NORDIC Signal Processing Symposium*, June 13-15, 2000, Kolmarden, Sweden, pp. 375-377.

[32] P. A. Fridman, "Interference Cancellation in Radio Astronomy Using Higher Order Statistics", *Proceedings of the ISSSE'01, 2001 URSI International Symposium on Signals, Systems, and Electronics*, July 24 - 47, 2001, Tokyo, Japan, pp. 196 - 199.

[33] P. A. Fridman, "Performance evaluation of sparse adaptive radio astronomy arrays", *Advanced Signal Processing Algorithms, Architectures and Implementation*, SPIE, v. 4474, pp.189-200, San-Diego, 31 July-3 Aug., 2001.

[34] The Square Kilometre Array, *http : //www.skatelescope.org*

[35] A. van Ardenne, B. Smolders, G. Hampson, "Active Adaptive Antennas for Radio Astronomy: Results for the R&D Program toward the Square Kilometre Array", in *Radio Telescopes*, ed. H. R. Butcher, SPIE, 4015, pp. 420-4337 (2000).

[36] Low Frequency Array, *http : //www.lofar.org*

[37] J. D. Bregman, "Concept Design for a Low Frequency Array", in *Radio Telescopes*, ed. H. R. Butcher, SPIE, 4015, pp. 19-33, (2000).

[38] P. J. Huber, *Robust Statistics*, New York: Wiley, 1981.

[39] T. P. Hettmansperger, *Statistical Inference Based on Ranks*, John Wiley & Sons, New York, 1984.

[40] F. R. Hampel, E. M. Ronchetti, P. J. Rousseeuw, W. A. Stahel, *Robust Statistics*, New York: Wiley, 1986.

[41] R. R. Wilcox, *Introduction to Robust Estimation and Hypothesis*, Academic Press, San Diego, 1997.

[42] A. M. Shurygin, *Applied Stochastics: Robustness, Estimation and Prediction*, Finances & Statistics, 2000.

[43] D. J. Sheskin, *Handbook of Parametric and Nonparametric Statistical Procedures*, Chapman & Hall/CRC, New York, 2000.